Controlled Synthesis of MnP Nanorods: Effect of Shape Anisotropy on Magnetization

Kristy A. Gregg,[†] Susanthri C. Perera,[†] Gavin Lawes,[‡] Samuel Shinozaki,[†] and Stephanie L. Brock*,[†]

Departments of Chemistry and Physics & Astronomy, Wayne State University, Detroit, Michigan 48202

Received September 15, 2005. Revised Manuscript Received December 14, 2005

Manganese phosphide (MnP) nanorods have been prepared by high-temperature injection of $Mn_2(CO)_{10}$ dissolved in octadecene into a hot (350 °C) surfactant mixture of trioctylphosphine oxide (TOPO) and trioctylphosphine (TOP). Uniform short rods (20.3 ± 3.6 nm × 5.2 ± 0.89 nm), grown along the *b* axis of orthorhombic MnP, were produced after 1 h of heating. The rods were ferromagnetic, with a coercive field of 4200 Oe at 10 K and a blocking temperature of 250.4 K at 500 Oe, and exhibited only weak interparticle interactions. Samples with longer rods having an aspect ratio of over 30 can be prepared by using longer heating times or multiple injections. The evolution of cubes and thicker rods was also observed with extended heating regimens. Surprisingly, the introduction of shape anisotropy into nanoparticles of MnP has little or no influence on the magnetic properties, suggesting that the inherent magnetocrystalline anisotropy is the dominating influence.

Introduction

Nanoscience is an integral component of several areas of technology, including such diverse fields as fuel and energy reform, information storage, catalysis, and medicine. This rapid development of nanotechnology is driven by the mantra of smaller equals faster, cheaper, and more efficient. The implementation of nanoparticulate materials in devices requires precise synthetic control of the size and shape of the nanoparticles, because the magnetic, electrical, and optical properties are dependent on these parameters.[1−3]

Many researchers have focused on creating one-dimensional nanomaterials (rods and wires) for use in practical applications such as sensing, electronics, and computer hard drives.[4] A wide range of one-dimensional materials, including metals, metal oxides, and metal chalcogenides, have been prepared, and their shape-dependent properties evaluated.[4−9] Magnetic materials, in particular, are desirable because of their potential use in magnetic data-storage devices,[10] site-specific drug release,[11] and magnetic refrigeration.[12] The shape anisotropy in one-dimensional ferromagnetic nanostructures can result in a significantly increased coercivity, which can be tuned by adjusting the aspect ratio.[2] Synthetic challenges remain in creating materials with uniform lengths and widths and specifically correlating the morphology with the resultant magnetic properties, as well as developing new chemistry to access more challenging phases.

Transition metal phosphides represent an exciting class of materials to explore on the nanoscale because of the wide range of properties exhibited in bulk materials. These include ferromagnetism, semiconductivity, and superconductivity, as well as catalytic activity.[13] However, only a few methodologies have been developed for targeting nanoscale transition metal phosphides. A solvothermal route has been implemented by Qian and co-workers and demonstrated for the production of CoP, Co_2P, Ni_2P, Cu_3P,[14] and FeP.[15] This method does not permit significant control over morphology and produces aggregated nanoparticles with a large degree of polydispersity. Lukehart and co-workers have created nanocomposites of several transition metal phosphides in silica xerogels, but the nanoparticles remained trapped in their host, which renders them unsuitable for further manipulation.[16,17] Likewise, transition metal phosphide nanoparticles including MoP, WP, Ni_2P, FeP, Fe_2P, and CoP have been

* To whom correspondence should be addressed. E-mail: sbrock@chem.wayne.edu.
[†] Department of Chemistry.
[‡] Department of Physics & Astronomy.

(1) Murray, C.; Sun, S.; Gaschler, W.; Doyle, H. *IBM J. Res. Dev.* **2001**, *45*, 47−56.
(2) Leslie-Pelecky, D. L.; Rieke, R. D. *Chem. Mater.* **1996**, *8*, 1770−1783.
(3) Alivisatos, A. P. *Science* **1996**, 271.
(4) Gao, J. G.; Bender, C. M.; Murphy, C. J. *Langmuir* **2003**, *19*, 9065−9070.
(5) Peng, X. M.; Manna, L.; Yang, W.; Wickham, J.; Scher, E.; Kadavanich, A.; Alivisatos, A. P. *Nature* **2000**, *404*, 59−61.
(6) Park, J. K.; Kang, E.; Bae, C. J.; Park, J.-G.; Noh, H.; Kim, J.-Y.; Park, J.-H.; Park, H. M.; Hyeon, T. *J. Phys. Chem. B.* **2004**, *108*, 13594−13598.
(7) Jun, Y.-W. J.; Jung, Y.-Y.; Cheon, J. *J. Am. Chem. Soc.* **2002**, *124*, 615−619.
(8) Joo, J.; Bin Na, H.; Yu, T.; Yu, J. H.; Kim, Y. W.; Wu, F.; Zhang, J. Z.; Hyeon, T. *J. Am. Chem. Soc.* **2003**, *125*, 11100−11105.
(9) Caswell, K. K.; Bender, C.; Murphy, C. J. *Nano Lett.* **2003**, *3*, 667−669.
(10) Spaldin, N. *Magnetic Materials*; Cambridge University Press: Cambridge, U.K., 2003.
(11) Lubbe, A.; Alexiou, C.; Bergemann, C. *J. Surg. Res.* **2001**, *95*, 200−206.
(12) Tegus, O.; Bruck, E.; Buschow, K. H. J.; de Boer, F. R. *Nature* **2002**, *415*, 150−152.
(13) Hullinger, F. *Struct. Bond.* **1968**, *4*, 83−229.
(14) Xie, Y.; Su, H. L.; Zian, X. F.; Liu, X. M.; Qian, Y. T. *J. Solid State Chem.* **2000**, *149*, 88−91.
(15) Yunle, G.; Fan, G.; Qian, Y. T.; Huangui, Z.; Ziping, Y. *Mater. Res. Bull.* **2002**, *37*, 1101−1105.
(16) Carpenter, J. P.; Lukehart, C. M.; Milne, S. B.; Stock, S. R.; Wittig, J. E.; Jones, B. D.; Glosser, R.; Zhu, J. G. *J. Organomet. Chem.* **1998**, *557*, 121−130.

10.1021/cm052080h CCC: $33.50
Published on Web 01/24/2006

synthesized by phosphate reduction, but supports are necessary to prevent aggregation.[18−23]

We have developed methodologies aimed at creating soluble (dispersible) transition metal pnictide nanoparticles with control of size and phase.[24,25] Iron phosphide nanoparticles were synthesized by treatment of Fe(III) salts with tris(trimethylsilyl)phosphine [$P(SiMe_3)_3$] in coordinating solvents. Magnetic studies conducted on 5-nm spherical FeP particles revealed Curie−Weiss paramagnetism down to 75 K.[19,24] Spherical, monodisperse MnP nanoparticles have been synthesized using either $P(SiMe_3)_3$ or trioctylphosphine (TOP) as the source of phosphorus and $Mn_2(CO)_{10}$ as the manganese source.[25] Although bulk manganese phosphide is ferromagnetic with a Curie temperature of $T_c = 292$ K and shows a metamagnetic transition to a modulated screw phase (T_N) at 47 K,[26] MnP spherical particles of 5.1 and 6.7 nm exhibited ferromagnetism over the entire temperature range below T_c, suggesting that the metamagnetic transition is suppressed in small crystallites. At 5 K, robust coercivities of 6000 Oe were observed, and the blocking temperature, T_b, scaled with size (increased size resulted in increased T_b), but all values were below 100 K.[25]

Recently, several groups have shown that trioctylphosphine (TOP) in a dual role as both a coordinating solvent and the source of phosphorus can produce metal phosphide nanorods. FeP nanorods have been made by a single high-temperature injection of iron carbonyl into a mixture of TOP and trioctylphosphine oxide (TOPO),[27,28] and Hyeon and co-workers have used a syringe-pump method to produce uniform nanorods of Fe_2P.[29] The Fe_2P rods were ferromagnetic and demonstrated an increase in both blocking temperature and coercive field with increasing aspect ratio. However, it was believed that the rods might contain a small amount of pure iron or a phase more iron-rich than Fe_2P, as the blocking temperatures (as high as 250 K) were greater than the T_c for Fe_2P (217 K).[29] In addition to Fe_2P, Hyeon and co-workers also recently published a general method employing a syringe pump to produce nanorods of MnP, Co_2P, FeP, and Ni_2P. The group cites the use of a syringe pump as a necessary condition for producing the rod shape, because of the continuously supplied precursor mixture. The magnetic properties of these materials were only briefly discussed, and the specific influence of shape anisotropy was not addressed, nor was the size dispersion for the rod samples reported.[30]

We have been investigating the role of TOP in the synthesis of MnP nanoparticles of varying size and shape. Nanorods are of particular interest because of the significant impact the shape anisotropy is expected to have on the magnetism of the ferromagnetic particles. The coercivity is expected to increase significantly with increasing aspect ratio, providing a mechanism to tune the resultant magnetic properties.[2,29,31] Additionally, as samples attain sizes where multiple domains are present, the low-temperature metamagnetic transition characteristic of bulk-phase MnP is expected to return. Here, we report the synthesis of MnP nanorods (20.3 ± 3.6 nm $\times$ 5.2 ± 0.89 nm) using simple manual injection of reagents and discuss the magnetic properties with respect to shape and magnetocrystalline anisotropy. Preliminary results on the formation of longer rods and other MnP nanoshapes are also presented.

Experimental Section

Synthesis. Reactions were conducted using air-free conditions employing a glovebox and a Schlenk line. Trioctylphosphine oxide (TOPO, Aldrich, 90%) was distilled before use. Trioctylphosphine (TOP, Strem, 97%), dimanganesedecacarbonyl [$Mn_2(CO)_{10}$, Strem, 98%], 1-octadecene (Aldrich, 90%), eicosane ($C_{20}H_{42}$, Acros, 99%), absolute ethanol (Pharmco, 200 proof), and chloroform (Fisher) were used without further purification.

Manganese phosphide nanorods were prepared using a high-temperature injection route. A 50:50 wt % mixture of TOP and TOPO, 6 mL and 5 g, respectively, was heated to 350 °C for approximately 2 h prior to the injection. The injection solution was composed of 0.74 mmol of $Mn_2(CO)_{10}$ in 7 mL of octadecene. This solution was heated to approximately 70 °C before being injected, at once via cannula, into the mixture of TOP and TOPO. Within 10−20 min, the solution turned black. The solution was then heated for an additional 1−5 h. For reactions with a lower-temperature postanneal, the temperature was reduced to 200−260 °C, and the solution was stirred for between 18 h and 2 days.

For reactions where another cannulated injection was made, the second injection was done between 45 min and 1 h after the initial injection at 350 °C. This injection solution contained additional TOP, compared to the first solution, to maintain the same ratio of Mn to TOP (1:18) in the reaction flask. The second injection was conducted at 280−320 °C, and the reaction mixture was stirred for between 30 min and 1 h, typically followed by a postanneal at 260 °C for 18 h.

The ratio of TOPO to TOP was also varied in some of the reactions to 10:90, 25:75, and 90:10 by weight. Injection of the Mn precursor/octadecene solution (7 mL, 0.106 M Mn) was again done at 350 °C. For ratios of 10:90 and 25:75, the mixtures were stirred for 1 h, whereas the 90:10 reaction mixture was heated for 6 h at 350 °C and then subjected to a low-temperature postanneal at 260 °C for 12 h.

Following heating, the nanoparticle solution was cooled to 60 °C by turning off the heating controller but leaving the flask on

(17) Burnam, K. J.; Carpenter, J. P.; Lukehart, C. M.; Milne, S. B.; Stock, S. R.; Jones, B. D.; Glosser, R.; Wittig, J. E. *Nanostruct. Mater.* **1995**, *5*, 155−169.
(18) Brock, S. L.; Perera, S. C.; Stamm, K. L. *Chem. Eur. J.* **2004**, *10*, 3364−3371.
(19) Stamm, K. L.; Garno, J. C.; Liu, G.-y.; Brock, S. L. *J. Am. Chem. Soc.* **2003**, *125*, 4038−4039.
(20) Sawhill, S. J.; Layman, K. A.; Van Wyk, D. R.; Engelhard, M. H.; Wang, C.; Bussell, M. E. *J. Catal.* **2005**, *231*, 300−313.
(21) Oyama, S. T. *J. Catal.* **2003**, *216*, 343−352.
(22) Zuzaniuk, V.; Prins, R. *J. Catal.* **2003**, *219*, 85−96.
(23) Phillips, D. C.; Sawhill, S. J.; Self, R.; Bussell, M. E. *J. Catal.* **2002**, *207*, 266−273.
(24) Perera, S. C.; Fodor, P.; Tsoi, G.; Wenger, L. E.; Brock, S. L. *Chem. Mater.* **2003**, *15*, 4034−4038.
(25) Perera, S. C.; Tsoi, G.; Wenger, L. E.; Brock, S. L. *J. Am. Chem. Soc.* **2003**, *125*, 13960−13961.
(26) Paduan-Filho, A.; Becerra, C. C. *J. Magn. Magn. Mater.* **2003**, *261*, 161−165.
(27) Chen, J.-H.; Tai, M.-F.; Chi, K.-M. *J. Mater. Chem.* **2004**, *14*, 296−298.
(28) Qian, C.; Kim, F.; Ma, L.; Tsui, F.; Yang, P.; Liu, J. *J. Am. Chem. Soc.* **2004**, *126*, 1195−1198.
(29) Park, J. K.; Koo, B.; Hwang, Y.; Bae, C. J.; An, K.; Park, J.-G.; Park, H. M.; Hyeon, T. *Angew. Chem., Int. Ed.* **2004**, *43*, 2282−2285.
(30) Park, J.; Koo, B.; Yoon, K. Y.; Hwang, Y.; Kang, M.; Park, J.-G.; Hyeon, T. *J. Am. Chem. Soc.* **2005**, *127*, 8433−8440.
(31) Park, S.-J.; Kim, S.; Lee, S.; Khim, Z. G.; Char, K.; Hyeon, T. *J. Am. Chem. Soc.* **2000**, *122*, 8581−8582.

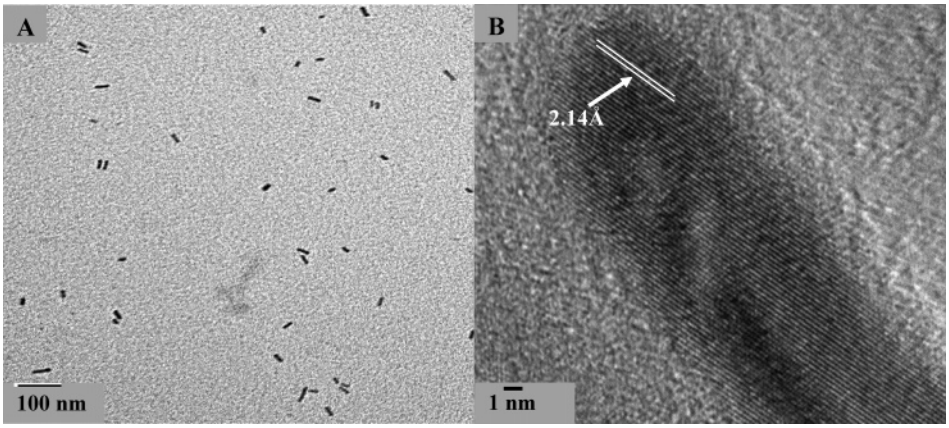

Figure 1. (A) Transmission electron micrograph of nanorods produced after 1 h of stirring at 350 °C. (B) Single-crystalline nanorod with lattice fringes corresponding to the (021) or (211) plane of MnP.

the heating mantle. Chloroform (10 mL) was added, and the resulting solution was stirred for approximately 30 min. Precipitation was achieved upon addition of 1−2 mL of absolute ethanol, and the resultant solid was isolated by centrifugation. All samples were stored under inert atmosphere in a glovebox. Attempts to isolate multiple fractions by treatment of the filtrate with more ethanol resulted in little or no precipitate formation.

X-ray Powder Diffraction (XRD). The X-ray powder diffraction patterns for all of the MnP samples were collected on a Rigaku Ru200B 12-kW diffractometer using Cu Kα radiation (1.54056 Å) at 40 kV and 150 mA. The precipitated MnP nanoparticles were deposited on a quartz (0001) low-background holder by smearing a small amount on the face of the plate.

Transmission Electron Microscopy (TEM). TEM images and electron diffraction patterns of the MnP nanoparticles were recorded using a JEOL FasTEM 2010 HR transmission electron microscope with a lanthanum hexaboride (LaB_6) thermoelectric emission gun operating at 200 kV. Samples were dispersed in pyridine, and one drop of the solution was placed on a 200-mesh carbon-coated copper TEM grid. The grid was left under inert ambient conditions for 1−2 h to evaporate the solvent.

Chemical Analysis. Quantitative analyses of Mn and P content were performed on the MnP nanorods. Samples were analyzed by Desert Analytics Laboratory (Tucson, AZ) using inductively coupled plasma-mass spectrometry (ICP-MS).

Magnetic Susceptibility. dc magnetic susceptibility studies were performed on the MnP nanorods using a Quantum Design model MPMS-5S SQUID magnetometer. Samples were sealed under vacuum in 15-cm-long quartz tubes prior to magnetic measurements to prevent air oxidation of the material. Magnetization versus field data were recorded at various temperatures in the range of 10−300 K, and magnetization versus temperature data were recorded on warming under applied fields in the range of 100−5000 Oe, after the sample had been cooled under either field-cooled (FC) or zero-field-cooled (ZFC) conditions. The samples were diluted using eicosane wax, on a weight percent basis. The dilutions examined included (eicosane/MnP): 50:50, 90:10, and 95:5.

Results

Synthesis. The synthesis of MnP nanorods involved a single high-temperature injection, in one portion, of a solution of $Mn_2(CO)_{10}$ dissolved in octadecene into a 50:50 wt % mixture of TOP and TOPO at 350 °C. In some cases, a second injection was performed (using the same concentration and volume of solution) 45 min later. TOP was used as the phosphorus source, as well as a coordinating cosolvent

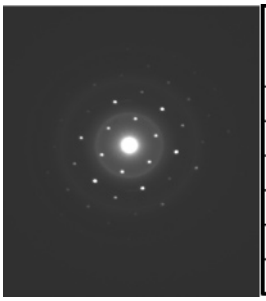

Measured d-spacing (Å)	d-spacing MnP (Å)	(hkl)
3.07	2.96	(200)
2.88	2.80	(101)
1.72	1.68	(130)
1.64	1.67	(301)
1.46	1.47	(112)
1.07	1.09	(340)

Figure 2. Electron diffraction of a single-crystal nanorod. The measured *d* spacings for the electron diffraction spots are listed in the table, as well as the *d* spacings reported for orthorhombic MnP and the corresponding (*hkl*) values.

in these reactions. Following the injection, a color change from yellow to black was observed, which took between 10 and 20 min. The length of heating time was varied (1−48 h), as was the temperature (350−260 °C) following the injection. The nanoparticles were isolated using a size-selective precipitation method; however, generally, only one fraction was obtained. The resultant precipitate was somewhat sticky in texture and was soluble in both chloroform and pyridine. Repeated washings yielded product with a more powdery consistency but reduced its solubility.

The ratio of TOPO to TOP was adjusted to 10:90, 25:75, and 90:10 by weight percent to observe the effects of the solvent composition on the resultant morphology. The 10:90 and 25:75 TOPO/TOP solutions were stirred for 1 h, whereas the 90:10 reaction mixture required longer times (6 h at 350 °C) for the color to change completely to black.

Structure and Morphology. Electron micrographs (Figure 1) show the rod morphology of the particles synthesized from a single injection after 1 h at 350 °C. The average particle size was determined statistically (Supporting Information) from TEM micrographs of >100 rods to be 20.3 ± 3.6 nm × 5.2 ± 0.89 nm with an average aspect ratio of 3.9. The average rod volume was determined to be 431 ± 166 nm^3, when modeled as a cylinder. The structure of an individual nanorod was determined using electron diffraction (ED) in the TEM instrument, and the measured *d* spacings can all be indexed on orthorhombic MnP (Figure 2). High-resolution images show lattice fringes that can likewise be indexed to MnP. Figure 1B shows a nanorod with lattice fringes corresponding to a *d* spacing value of 2.14 Å, which can be

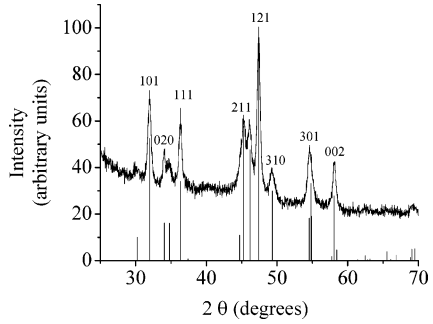

Figure 3. Typical powder XRD pattern for MnP nanorods. The peaks correspond to a library match to PDF 78-0267 (MnP), as shown by the line diagram.

indexed to the (021) or (211) reflection of MnP, oriented approximately 20° from the growth direction of the rod. Typically, the fringes are found to be parallel to the axial direction of the rod, in which case they can be indexed to the (200) or (101) reflections (Supporting Information). Powder XRD patterns of nanoparticle samples are consistent with the TEM/ED data, yielding patterns consistent with crystalline orthorhombic MnP, as shown in a typical XRD pattern for MnP nanorods in Figure 3. No additional peaks were observed.

MnP samples produced from a single injection and isolated after being heated for 4.5 h at 350 °C consisted of a mixture of longer rods with aspect ratios above 30, shorter rods, rectangles, and cubes, as shown in Figure 4A. When two injections were employed, followed by a low-temperature postanneal (260 °C, 18 h), the samples were composed of longer rods with aspect ratios of >30, along with shorter rods, as shown in Figure 4B. Samples prepared using a single precursor injection, followed by heating at 350 °C for 15 min and then at 260 °C for 2 days, showed a mixture consisting mostly of cubes and short rods, as illustrated in Figure 5. Varying the ratio of TOPO to TOP to 10:90, 25:75, and 90:10 resulted in polydisperse samples consisting of a variety of nanoshapes including rods, cubes, and spheres (Supporting Information). The rods observed were approximately 20−50 nm in length and 5−7 nm in width. All of the samples had XRD patterns consistent with orthorhombic MnP formation.

Magnetic Properties. Magnetic measurements (Figure 6) were performed on several short-rod samples, with similar results obtained in all cases. The TEM image for a 20.3 × 5.2 nm short-rod sample is shown in Figure 1A. Hysteresis loops are present in the magnetization versus field graph (Figure 6A), consistent with the ferromagnetic behavior of nanoparticles, and diminish in width with increasing temperature. The coercivity (H_c) is 4200 Oe at 10 K and decreases to 500 Oe at 250 K. Saturation behavior is retained up to 275 K (at which point $H_c = 0$), and by 300 K, the sample exhibits paramagnetic behavior. The rods had a saturation magnetization (M_s) of 9950 emu/mol, determined by extrapolating the data to infinite field on a magnetization versus inverse field graph.

Figure 6B shows the magnetization versus temperature data conducted on samples cooled in the presence (FC) and absence (ZFC) of the measuring magnetic field. The FC data show a transition near 300 K that exhibits only a small field dependence. The ZFC data deviate from the FC data at lower temperature, exhibiting a maximum and then decreasing toward zero. The temperature at which this maximum occurs is the blocking temperature (T_b) and is field-dependent, decreasing from 254.4 K at 100 Oe to 210.4 K at 2500 Oe.

Measurements were also conducted on a series of samples diluted in wax (eicosane). The effect of dilution on T_b is presented in Table 1. Only a small (but monotonic) decrease in T_b is observed when the nanoparticle sample ($T_b = 242.4$ K) is diluted to 5% ($T_b = 235.5$ K) by weight.

Discussion

To correlate the magnetic properties of a nanomaterial with the morphology, uniform samples must be available. There has been one recent report of MnP nanorods in the literature by Hyeon and co-workers, and it is based on the reaction of $Mn_2(CO)_{10}$ with the phosphorus source TOP.[30] The rods were produced using an injection method employing a syringe pump that provided a continuous supply of precursor solution, and both the syringe pump and a combination of TOP and TOPO surfactants were deemed necessary for rod formation. Hyeon and co-workers found that there was a critical precursor concentration that needed to be exceeded before nucleation of their MnP nanorods would occur.[30] The rate at which this threshold concentration was achieved directly influenced the length of the rods they were able to synthesize (faster injection rates yielded longer rods) up to an aspect ratio of 3.67. However, no statistical data were reported on the length/width of the rods, and the TEM images revealed inconsistencies in the rod shapes, as well as the presence of cubes and some hexagon-shaped particles.[30]

In this work, the synthesis of short nanorods (20.3 ± 3.6 nm × 5.2 ± 0.89 nm, aspect ratio = 3.9) was achieved with a single high-temperature injection of the manganese precursor into the surfactant mixture. The injection had to be done at ≥350 °C for nucleation of the particles to occur rapidly, as evidenced by a change in color to orange and then black. At lower temperatures, the reaction either failed (no color change occurred, and no particles precipitated from the reaction) or took several hours to go to completion. Size-selective precipitation was attempted using a solvent system of chloroform and ethanol, but typically, only one fraction could be isolated. If more than one fraction was precipitated, when analyzed, these fractions were typically indistinguishable with respect to the size and shape distributions of the nanoparticles. Additionally, TEM samples prepared from synthesis solutions prior to isolation revealed similar distributions of particle sizes and shapes, suggesting that the isolated samples were reflective of the as-prepared nanoparticles. All samples were stored in an inert atmosphere, because if left in air, they lost their crystallinity (as revealed by XRD and TEM), possibly because of oxidation.

Effect of Heating Time and Multiple Injections. The synthesis of MnP nanorods with higher aspect ratios was achieved by two methods: increased heating time and the use of multiple injections of precursor materials, both employing 50:50 mixtures of TOPO/TOP. With increased heating time, rod and wire growth occurred but was not uniform, as shown in Figure 4A. Additionally, cubes and

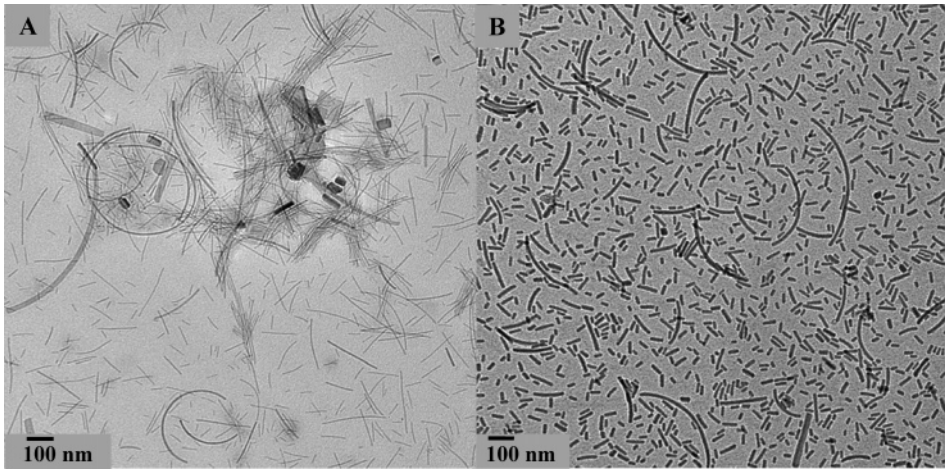

Figure 4. TEM images of nanorods produced (A) after 4.5 h of stirring at 350 °C and (B) after a second precursor injection at 320 °C conducted 45 min after the 350 °C injection, 30 min of stirring, and then 18 h of postannealing at 260 °C

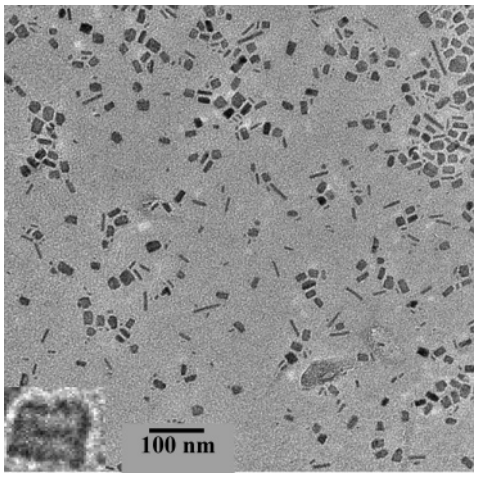

Figure 5. TEM image showing the appearance of cubes after 15 min of heating at 350 °C followed by 2 days of heating at 260 °C. The enlarged inset shows what appear to be two rectangular particles merging to form a cube.

rectangular shapes were observed. The nonuniform growth of the nanorods is possibly due to Ostwald ripening, attributed to an insufficient amount of monomers available for growth in solution. As nanoparticles grow, the monomer concentration is steadily diminished, and the solution approaches a critical concentration. At this point, the smaller nanoparticles become soluble, and the larger particles continue to grow, according to the Gibbs−Thompson law.[32] Multiple injections were attempted to maintain a high monomer concentration, which has been reported to aid in uniform rod growth of CdSe and InAs.[32,33] A second injection, conducted 45 min after the first injection, was partially successful, producing rod samples with a narrow polydispersity in widths and no other shapes (Figure 4B). However, the axial growth did not appear to occur uniformly, and a variety of lengths, yielding aspect ratios up to 33, were achieved.

Effect of TOPO/TOP Ratio. The ratio of TOPO to TOP in these reactions is an important factor in maintaining a one-dimensional shape. Both the Hyeon group[30] and Liu and co-workers[28] employed similar surfactant mixtures to achieve nanorods of transition metal phosphides. The use of multiple surfactants that have different binding properties is well-known to lead to the formation of anisotropic shapes by inhibiting growth along some crystal faces. This technique can be coupled with a high monomer concentration to achieve morphological control.[8,28,32,34] The TOPO/TOP concentration was varied to 10:90, 25:75, and 90:10 by weight percentage, and the TEM images showed the appearance of multiple shapes, including cubes and spheres, in each case (Supporting Information). We also examined a reaction performed without TOPO (pure TOP) and saw mostly spheres with very few rods. The reaction mixtures containing a higher concentration of TOP generally showed rapid nucleation following the injection, whereas those with more TOPO were much slower to nucleate and required much longer heating times. For the ratios of 10:90 and 25:75, the reaction mixtures were stirred for 1 h at 350 °C. The 90:10 reaction mixture, however, required 6 h at 350 °C followed by 12 h at 260 °C for the reaction to go to completion, as evidenced by a color change to deep black. We surmise that this reaction is kinetically slower because we are limiting not only one of the surfactants, but also a reactant, because of the dual role TOP plays in these reactions. As with reactions involving a 50:50 wt % mixture of TOPO/TOP, the process must take place at 350 °C for nucleation to occur reliably and the reaction to proceed. Lower temperatures typically result in reaction failure, which again was indicated by a lack of color change, or the inability to precipitate particles. On the basis of these findings, we believe that maintaining the 50:50 wt % mixture of TOPO/TOP is important to maintaining a one-dimensional shape, as previously noted by Hyeon and co-workers[30] and Liu et al.[28]

Effect of Postannealing Conditions. The formation of other shapes, including cubes and thicker rods, was achieved by varying both time and temperature following injection into the TOPO/TOP mixture. As mentioned previously, in addition to increasing the aspect ratio of the rods, increased heating times resulted in the appearance of thicker rods and cubes (Figure 4A). To maximize cube formation, extensive

(32) Peng, Z. A.; Peng, X. G. *J. Am. Chem. Soc.* **2001**, *123*, 1389−1395.
(33) Peng, X.; Wickham, J.; Alivisatos, A. P. *J. Am. Chem. Soc.* **1998**, *120*, 5343−5344.
(34) Manna, L.; Scher, E. C.; Alivisatos, A. P. *J. Am. Chem. Soc.* **2000**, *122*, 12700−12706.

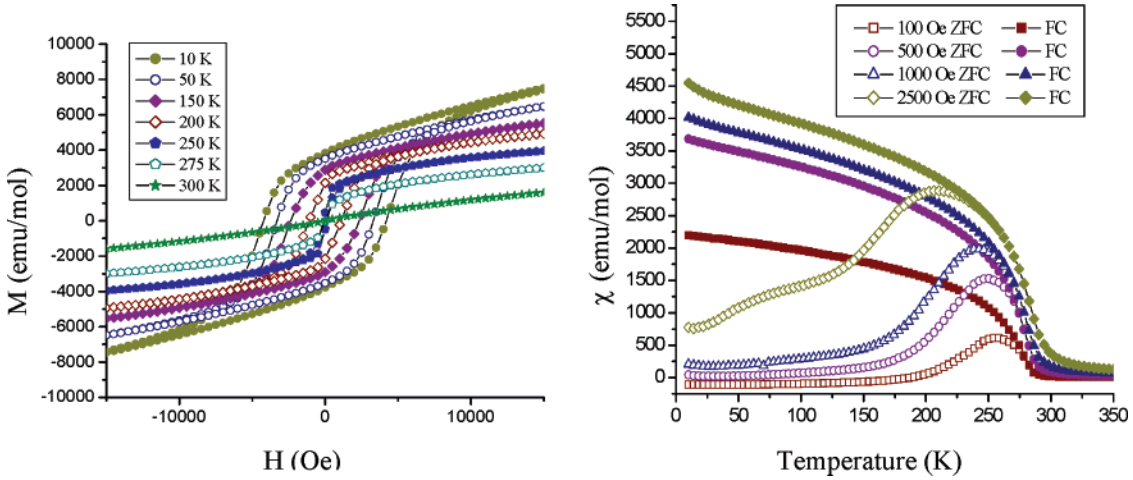

Figure 6. Magnetic data for the MnP 20.3 × 5.2 nm rod sample. (A) Magnetization versus field graph for temperatures varying from 10 to 300 K. (B) Zero-field-cooled (ZFC) and field-cooled (FC) susceptibility data acquired at applied fields varying from 100 to 2500 Oe.

Table 1. Magnetic Data Collected at 1000 Oe Following Systematic Weight Percent Dilutions of the 20.3 × 5.2 MnP Nanorods with Eicosane

wt % of MnP	blocking temp (K)
100	242.4
50	238.4
10	237.5
5	235.5

postannealing at temperatures lower than the nucleation temperature is required. We observed the emergence of many cubes by heating at 350 °C for 15 min and then postannealing at 260 °C for 2 days. The increase in the number of cubes was significant compared to samples heated for shorter times (4.5 h) at the nucleation temperature, as is evidenced by comparing Figure 5 with Figure 4A. Heating samples for longer than 4.5 h at 350 °C produced very large rods (lengths up to microns). In several cases, we also observed what appeared to be the merging of rectangular particles or rods together to form these cubes, which we believe might provide a possible explanation for this shape evolution. The TEM images show a dark line between some of these particles, shown in the inset in Figure 5. There have been several reports of oriented attachment of nanoparticles to form nanorods in the literature,[35,36] and the rod-to-cube transformation noted here might be yet another example. As with the pure nanorod samples, size-selective precipitation was attempted, but generally, only one fraction was produced, and we were unable to separate the cubes/rectangles from the rods.

Effect of Shape on Magnetic Properties. To ascertain the role of shape anisotropy on magnetic property development in MnP, we conducted a comparison of the magnetic properties of previously synthesized 6.7-nm spheres[25] of MnP and the 20.3 × 5.2 nm rods of MnP (aspect ratio = 3.9) reported here. We anticipated augmentation of the coercivity and blocking temperature in the rods relative to the spheres because of shape-anisotropy contributions to the magnetism that arise from demagnetization effects. Furthermore, because of the increased volume of the rods relative to the spheres, we also considered the possibility that the metamagnetic transition ($T_N \approx 50$ K) observed in bulk samples would reemerge.

In examining the magnetization versus temperature data (Figure 6B), we observed a much higher blocking temperature, indicated by the maximum in the ZFC data, for the rods versus the spheres. The blocking temperature is the point above which the particles become superparamagnetic (i.e., the moments can thermally relax within the sampling time of the instrument). This can also be detected by the absence of hysteresis in the magnetization versus field data. At 500 Oe, the blocking temperature (T_b) was determined to be 250.4 K. This was similar to the blocking temperature reported by Hyeon and co-workers[30] for 11 × 25 nm MnP rods (T_b = 260 K, 100 Oe), whereas the 6.7-nm MnP spheres showed a T_b of 74.3 K (500 Oe). The rods had an extrapolated saturation magnetization of 9950 emu/mol (636 emu/cm^3), which is reasonably close to that determined for 6.7-nm MnP spheres at 8950 emu/mol (572 emu/cm^3). If one neglects surface spin effects, the saturation magnetization is an intrinsic property of the material and is not expected to vary significantly with shape/size. The consistency among the various data sets suggests that the particles are not contaminated by other ferromagnetic phases. No evidence for the reemergence of metamagnetism (which would show an anomaly in the M vs T curves at the Néel temperature of approximately 50 K) was observed in any of the data. This suggests that the increase in particle size still had not reached a critical length scale where the large magnetic cell for the metamagnetic state (ca. 2.8 nm along c) is stabilized.[37]

The blocking temperature T_b can depend on interparticle interactions,[38−40] which might be expected to vary with morphology. Thus, before comparing the magnetic properties of nanorods and nanospheres, it is first necessary to investigate the possible contributions from interparticle interactions. To examine the effect of particle−particle interac-

(35) Tang, Z.; Kotov, N. A.; Giersig, M. *Science* **2002**, *297*, 237−240.
(36) Cho, K.-S.; Talapin, D. V.; Gaschler, W.; Murray, C. B. *J. Am. Chem. Soc.* **2005**, *127*, 7140−7147.
(37) Huber, E. E., Jr.; Ridgley, D. H. *Phys. Rev.* **1964**, *135*, A1033−A1040.
(38) El-Hilo, M.; O'Grady, K.; Chantrell, R. W. *J. Magn. Magn. Mater.* **1992**, *114*, 295−306.
(39) Farrell, D.; Cheng, Y.; McCallum, R. W.; Sachan, M.; Majetich, S. A. *J. Phys. Chem. B* **2005**, *109*, 13409−13419.
(40) Vestal, C. R.; Song, Q.; Zhang, Z. J. *J. Phys. Chem. B* **2004**, *108*, 18222−18227.

tions on the magnetic properties, we systematically diluted the MnP nanorods with eicosane. We observed a small but definite trend in the blocking temperature as a function of nanoparticle concentration: As the sample became more dilute, the blocking temperature decreased (Table 1). However, the overall shift in blocking temperature is very small, suggesting that interparticle interactions play only a minimal role in determining the magnetic properties of this nanorod system; changing the particle concentration by a factor of 20 changes the blocking temperature by less than 3%.

The T_b behavior can be modeled for single-domain particles by the Stoner−Wohlfarth equation (eq 1), where E is the anisotropy energy; K is the uniaxial anisotropy constant; θ is the angle between the net nanoparticle moment and the magnetic easy axis; V is the nanoparticle volume; k_B is the Boltzmann constant; T_b is the blocking temperature; and $\ln(t/\tau_0)$ is approximately 25 for dc magnetic measurements, assuming a typical microscopic time scale of $\tau_0 = 10^{-9}$s.[41]

$$E = KV \sin^2 \theta = k_B T_b \ln(t/\tau_0) \quad (1)$$

Equation 1 shows that, as the volume of the nanoparticle increases, so does the anisotropy energy and, thus, the blocking temperature. The average volume for a rod was determined to be 431 ± 166 nm^3 compared to 155 ± 23 nm^3 for the ca. 6.7-nm sphere sample. The larger volume of the rods directly increases the total anisotropy energy, thus leading to a much higher blocking temperature than observed for the spheres.

Examination of the magnetization vs field data reveals that the coercivity of the nanorods, rather than being augmented, is actually less than that for spheres (4200 Oe at 10 K vs 5000 Oe for 6.7-nm spheres). As previously stated, the introduction of shape anisotropy (spheres-to-rods) should ideally result in an increased coercivity. For example, a study conducted by Zurcher and co-workers on ferromagnetic cobalt nanospheres and nanorods showed a significant increase in coercivity with increased aspect ratio. The coercivity changes from 1100 Oe for their 3-nm spheres to 8900 Oe for their 9 × 40 nm rods (aspect ratio = 4.44).[42] This unexpected decrease in coercivity in MnP nanorods is also observed in the data of Hyeon and co-workers, who reported a coercivity of 5000 Oe at 15 K for rods of dimension 11 × 25 nm (aspect ratio = 2.27).[30]

To explore this discrepancy, we calculated the effective anisotropy constants (K) for both the spheres and the rods. In principle, the introduction of shape anisotropy should result in an increase in K over the value obtained for spheres.[31] In practice, materials with small saturation magnetizations (M_s) can be expected to show little or no shape dependence, because the contribution to the magnetic anisotropy arising from shape depends on M_s^2. Because the M_s value for MnP is similar (in fact larger) than the value for Ni (M_s = 485 emu/cm^3), which does show significant shape

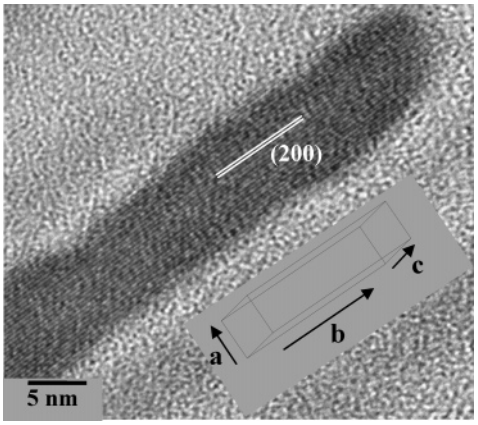

Figure 7. High-resolution TEM image of a MnP nanorod with lattice fringes corresponding to the (200) plane. The *a*, *b*, and *c* axes of the MnP unit cell are labeled on the rod and correspond to the hard, intermediate, and easy axes, respectively, according to the preferred magnetic direction the spins align. The *c* axis goes into the plane of the paper.

dependence,[43] we do expect to see clear differences in the anisotropy constants calculated for rods vs spheres. The uniaxial anisotropy constant can be estimated for superparamagnetic particles using eq 1. Using the measured values of the blocking temperature for the nanorods and nanospheres, together with the estimated volumes, we find that the effective anisotropy constant for the spherical nanoparticles is similar to that for the nanorods, 1.65 × 10^6 ± 2.4 × 10^5 erg/cm^3 versus 2.0 × 10^6 ± 7.7 × 10^5 erg/cm^3. Likewise, the anisotropy constant can be determined from the coercive field, H_c, using eq 2, where $\alpha = 0.48$ (a numerical prefactor appropriate for randomly oriented particles). K_{eff} includes a contribution from the magnetocrystalline anisotropy as well as from the shape anisotropy.

$$H_c = \alpha (2K_{eff}/M_s) [1 - (T/T_b)^{1/2}] \quad (2)$$

Comparing data for spheres and rods at $T = 10$ K, we find that, although quantitatively different from values obtained with eq 1, the K values for spheres and rods are again very similar: 4.70 × 10^6 and 3.48 × 10^6 erg/cm^3, respectively. Thus, the introduction of shape anisotropy has very little influence on the overall magnetic anisotropy of the system.

A possible explanation for this effect becomes apparent upon examination of the rods using high-resolution TEM. MnP has an orthorhombic structure with lattice parameters of 5.92, 5.25, and 3.17 Å, following the convention $a > b > c$ proposed by Rundqvist et al.[44] The high-resolution images of several rods (Figure 7 and Supporting Information) suggest that the growth direction is along the *b* axis, based on the fact that fringes parallel to the growth axis cannot be indexed to reflections with a nonzero *k* index [i.e., all are (*h*0*l*) or (*h*00) reflections]. Likewise, fringes that are not collinear with the growth direction can be indexed to either (0*kl*) or (*hkl*) reflections (Figure 1B and Supporting Information). The X-ray diffraction patterns provide further confirmation (Figure 3). If the growth were random, one would

(41) Stoner, E. C.; Wohlfarth, E. P., *Philos. Trans. R. Soc. A* **1948**, *240*, 599−642.
(42) Dumestre, F.; Chaudret, B.; Amiens, C.; Fromen, M.-C.; Casanove, M.-J.; Renaud, P.; Zurcher, P. *Angew. Chem., Int. Ed.* **2002**, *41*, 4286−4289.
(43) Sellmyer, D. J.; Zheng, M.; Skomski, R. *J. Phys.: Condens. Matter* **2001**, *13*, R433−R460.
(44) Rundqvist, S.; Nawapong, P. C. *Acta Chem. Scand.* **1965**, *19*, 1006−1007.

expect uniform broadness of the XRD peaks, reflecting the average nanoscale dimensions of the crystallites, as observed for spherical nanoparticles of MnP;[25] however, the (020) reflection is much sharper than the other reflections, indicating that the crystallite dimensions along *b* are greater than those along *a* and *c*. According to the literature, the easy magnetic axis (the axis along which the spins prefer to align) in bulk MnP is the *c* axis, whereas the *b* axis is intermediate, and the *a* axis is hard.[26] Thus, as illustrated in Figure 7, the magnetocrystalline easy axis (*c* axis) does not fall along the preferred moment direction arising from the shape anisotropy (*b* axis). This might give rise to a competition between magnetocrystalline and shape anisotropy in the nanorods resulting in a *reduction* of the effective anisotropy in these nanoparticles and, thus, very similar coercivities and anisotropy constants for the spheres and the rods. If the rods were grown along the easy magnetic axis, the shape anisotropy might be expected to become a more dominant phenomenon.

Alternatively, the magnetic anisotropy in this system might be dominated by the intrinsic lattice magnetocrystalline anisotropy, with only a minor contribution (if any) by shape anisotropy. In this case, even growth along the easy magnetic axis (*c*) would be expected to have little or no effect. In fact, this supposition has been tested. Hyeon and co-workers noted that the growth direction of MnP rods prepared by continuous precursor injection is perpendicular to the (002) lattice fringes that they observed, i.e., along *c*.[30] The fact that they observe a similar coercivity for their rods (grown along the easy magnetic axis, *c*) as compared to ours (grown along the intermediate magnetic axis, *b*) strongly suggests that shape anisotropy is a minor contributor to the magnetic behavior of MnP nanoparticles. It remains an open question as to why the shape anisotropy does not affect the magnetic properties of MnP more dramatically. It might be important to investigate the effects of surface spins to properly address this problem.

Conclusions

A reproducible method based on a single, quick injection of precursors into mixed surfactants to make short, uniform nanorods of MnP (aspect ratio = 3.9) has been developed. Through adjustment of heating temperature and time, rods can be produced with uniform widths and aspect ratios of up to 33. In contrast to a previously reported MnP nanorod synthesis, the rods grow along the *b* axis, rather than the *c* axis, and short-rod samples can be generated that have narrower polydispersities and higher aspect ratios. Through a comparison with spherical nanoparticles and data for rods grown along the magnetically easy *c* axis, it appears that the inherent magnetocrystalline anisotropy in this system dominates the magnetic interactions; introduction of shape anisotropy has little or no influence on the observed properties. In addition to rod formation, other shapes, most notably nanocubes, can be produced in the MnP system by the use of low-temperature postannealing. Our current work is focused on investigating the mechanism of formation and magnetic properties of these cubes.

Acknowledgment. We thank Professor Lowell E. Wenger and Dr. Georgy Tsoi for acquiring preliminary magnetism data. Acknowledgment is made to the National Science Foundation (CAREER award DMR-0094273 and IGERT-970952) for financial support of this research.

Note Added after ASAP Publication. The wrong received date was listed in the version published ASAP January 24, 2006; the corrected version was published ASAP February 1, 2006.

Supporting Information Available: Transmission electron micrographs for samples produced by varying the surfactant ratio of TOP to TOPO, size distribution histograms for the 20.3 ± 3.6 nm $\times$ 5.2 ± 0.89 nm MnP nanorods, HRTEM image of a MnP nanorod, and growth direction calculations. This material is available free of charge via the Internet at http://pubs.acs.org.

CM052080H